Repurposing Ceritinib Induces DNA Damage and Enhances PARP Inhibitor Responses in High-Grade Serous Ovarian Carcinoma

Arun Kanakkanthara[1,2], Xiaonan Hou[1], Thomas L. Ekstrom[1], Valentina Zanfagnin[1], Amelia M. Huehls[1], Rebecca L. Kelly[2], Husheng Ding[1], Melissa C. Larson[3], George Vasmatzis[4], Ann L. Oberg[5], Scott H. Kaufmann[1,2], Aaron S. Mansfield[1], S. John Weroha[1], and Larry M. Karnitz[1,2]

ABSTRACT

PARP inhibitors (PARPi) have activity in homologous recombination (HR) repair-deficient, high-grade serous ovarian cancers (HGSOC). However, even responsive tumors develop PARPi resistance, highlighting the need to delay or prevent the appearance of PARPi resistance. Here, we showed that the ALK kinase inhibitor ceritinib synergizes with PARPis by inhibiting complex I of the mitochondrial electron transport chain, which increases production of reactive oxygen species (ROS) and subsequent induction of oxidative DNA damage that is repaired in a PARP-dependent manner. In addition, combined treatment with ceritinib and PARPi synergized in HGSOC cell lines irrespective of HR status, and a combination of ceritinib with the PARPi olaparib induced tumor regression more effectively than olaparib alone in HGSOC patient-derived xenograft (PDX) models. Notably, the ceritinib and olaparib combination was most effective in PDX models with preexisting PARPi sensitivity and was well tolerated. These findings unveil suppression of mitochondrial respiration, accumulation of ROS, and subsequent induction of DNA damage as novel effects of ceritinib. They also suggest that the ceritinib and PARPi combination warrants further investigation as a means to enhance PARPi activity in HGSOC, particularly in tumors with preexisting HR defects.

Significance: The kinase inhibitor ceritinib synergizes with PARPi to induce tumor regression in ovarian cancer models, suggesting that ceritinib combined with PARPi may be an effective strategy for treating ovarian cancer.

Introduction

High-grade serous ovarian cancer (HGSOC), which accounts for over 70% of all ovarian cancer cases, remains the most lethal gynecologic malignancy. The disease is usually diagnosed at an advanced stage and, despite advances in understanding HGSOC biology, is still associated with 5-year survival of approximately 30% (1). Approximately 50% of all HGSOCs harbor defects in homologous recombination (HR) DNA repair due to mutations in or epigenetic silencing of *BRCA1*, *BRCA2*, *RAD51C*, and other HR genes (2). Notably, the HR deficiency (HRD) in these tumors is associated with a better response to platinum-based chemotherapy and thus with a better clinical outcome, likely because platinum induces DNA lesions that are repaired, in part, by HR (3). However, most HR dysfunctional tumors eventually acquire resistance to platinum after an initial complete response (4), highlighting the need for better treatment options for the management of HGSOCs.

Defects in HR also confer sensitivity to PARP1 and PARP2 inhibitors (PARPi; ref. 3). PARP1/2 (hereafter referred to as PARP) participates in multiple DNA repair pathways, including the base excision repair (BER) pathway that corrects small base modifications and single-strand breaks (5). PARPis have the greatest activity in HR-deficient cells, where the HR repair defect causes increased sensitivity to double-stranded DNA breaks and possibly other lesions induced by PARP inhibition or trapping (6, 7). Notably, these agents have emerged as important therapies for HGSOCs in the frontline setting as maintenance therapy and in the recurrent setting following platinum-based therapy (6). However, complete responses to PARPi monotherapy are rare, and partial responses are more common for recurrent disease, even with *BRCA1/2* mutation (8–10). Furthermore, the clinical benefits of PARPi therapy in HR-proficient HGSOCs (which account for about 50% of HGSOCs) are of borderline significance (6, 11). Accordingly, despite recent progress in treating HGSOC, novel therapeutic approaches are needed.

In the present study, we examined the effect of ceritinib on HGSOC. Ceritinib is a small-molecule kinase inhibitor that is approved as first-line therapy for non–small cell lung cancer (NSCLC) with rearrangement of *ALK*, an oncogenic tyrosine kinase in this disease (12, 13). These studies were initiated on the basis of our observation that *ALK* is amplified and mutated in a small subset of HGSOC, raising the possibility that ALK inhibitors may have activity in HGSOC. However, we found that ceritinib did not have single-agent activity in HGSOC patient-derived xenograft (PDX) mouse models with increased *ALK* alterations or ALK overexpression. Instead, ceritinib synergized with

[1]Department of Oncology, Mayo Clinic, Rochester, Minnesota. [2]Department of Molecular Pharmacology and Experimental Therapeutics, Mayo Clinic, Rochester, Minnesota. [3]Department of Quantitative Health Sciences, Division of Clinical Trials and Biostatistics, Mayo Clinic, Rochester, Minnesota. [4]Center for Individualized Medicine, Mayo Clinic, Rochester, Minnesota. [5]Department of Quantitative Health Sciences, Division of Computational Biology, Mayo Clinic, Rochester, Minnesota.

Corresponding Authors: Larry M. Karnitz, Mayo Clinic, 200 First Street SW, Rochester, MN 55905. Phone: 507-284-3124; E-mail: karnitz.larry@mayo.edu; S. John Weroha, Weroha.Saravut@mayo.edu; and Arun Kanakkanthara, Kanakkanthara.Arun@mayo.edu

Cancer Res 2022;82:307–19

doi: 10.1158/0008-5472.CAN-21-0732

PARPis in ovarian cancer cell lines, and a ceritinib + PARPi combination had greater activity than either drug alone in HGSOC PDX mouse models *in vivo*, especially in models with preexisting PARPi sensitivity. Mechanistic analyses revealed that ceritinib did not synergize with PARPis by disrupting HR or by inhibiting other kinases that are known ceritinib targets. Instead, ceritinib inhibited complex I in the mitochondrial electron transport chain, leading to the production of reactive oxygen species (ROS) and consequent induction of DNA damage that is repaired in PARP-assisted repair pathways, including BER. Consistent with the ability of ceritinib to induce DNA damage that is repaired in a PARP-dependent manner, addition of PARPi, which disrupts the BER/single-strand break DNA repair pathway, synergized with ceritinib. These findings provide preclinical evidence that supports possible repurposing of ceritinib to enhance the responses to PARPis in HGSOCs.

Materials and Methods

Cell lines, cell culture, and drugs

HR-proficient OVCAR-8 (D. Scudiero, National Cancer Institute) and OVCAR-8-DR-GFP cells (14), the *BRCA1*-mutant COV362 cells (Robert van Waardenburg, University of Alabama at Birmingham, Birmingham, AL), prostate cancer PC3 (Haojie Huang, Mayo Clinic), and breast cancer MDA-MB-231 cells (Zhenkun Lou, Mayo Clinic) were cultured in RPMI-1640 media (Corning) supplemented with 8% FBS (Millipore) and maintained in a humidified 5% CO_2 incubator at 37°C. All cells were authenticated by autosomal STR profiling (University of Arizona Genetics Core) and were free of *Mycoplasma* contamination as determined by testing with a MycoAlert *Mycoplasma* Detection Kit (catalog no. LT07-118, Lonza) every 6 months. Cell lines were reinitiated from cryopreserved stocks every 3 to 6 months.

Ceritinib used for cell culture experiments as well as olaparib, veliparib, IACS-010759, and linsitinib were obtained from Selleck Chemicals. The ceritinib used for mouse studies was provided by Novartis. Cisplatin was obtained from Teva Pharmaceutical Industries. SL0101 was purchased from Millipore.

siRNAs and siRNA transfection

All siRNAs were purchased from Dharmacon. For siRNA transfections, 8×10^6 cells were suspended in 180 μL complete growth medium and 20 μL of 20 μmol/L siRNA were electroporated using a BTX ECM 830 electroporator using two 280-volt, 10-msec pulses. Transfections were repeated once after 24 hours, and cells were used for experiments 48 hours after the second transfection. siRNAs used were:

siLuciferase, 5′-CUUACGCUGAGUACUUCGA-3′;
siXRCC1 #1, 5′-GGGAAGAGGAAGUUGGAUU-3′;
siXRCC1 #2, 5′-CUCGACUCACUGUGCAGAA-3′.

The following genes were targeted with siGENOME SMARTpool siRNAs (Dharmacon/Horizon Discovery) that contain a pool of four different siRNAs that target various regions of each gene: RAD51C (catalog no. M-010534-01), ALK (catalog no. M-003103-02), CAMKK2 (catalog no. M-004842-02), EGFR (catalog no. M-003114-03), FLT3 (catalog no. M-003137-02), FER (catalog no. M-003129-02), FES (catalog no. M-003130-01), FAK (catalog no. M-003164-02), and ROS1 (catalog no. M-003173-01).

Colony formation assays

OVCAR-8 (300 cells per well), COV362 (300 cells per well), PC3 (750 cells per well), or MDA-MB-231 (700 cells per well) cells were plated in 6-well plates in triplicate and incubated overnight. The cells were then treated with vehicle or various concentrations of compounds as indicated and cultured for 8–10 days in the continued presence of agents. Colonies were stained with Coomassie Brilliant Blue and counted manually. Survival was expressed as a percentage of the control with no drug treatment. Combination index values were calculated by the Chou–Talalay method (15) using CalcuSyn software (Biosoft). For colony formation assays involving siRNA-mediated knockdown, cells were plated at the following densities: 450 cells/well for siRAD51C and 300 cells/well for all other siRNAs.

Seahorse assay

OVCAR-8 or COV362 cells were plated at 6,000 or 4,000 cells per well, respectively, in Seahorse 8-well XFp cell culture miniplates and allowed to grow for 24 hours. The cells were then treated with vehicle or indicated concentrations of ceritinib, olaparib, or ceritinib + olaparib for 12 hours and assayed for oxygen consumption rate (OCR) and extracellular acidification rate on a Seahorse XFp extracellular flux analyzer (Seahorse Bioscience, Agilent Technologies) as described previously (16). To measure the effect of ceritinib on different mitochondrial electron transport chain complexes, OVCAR-8 cells (8,000 cells per well) were seeded in and cultured overnight in Seahorse 8-well XFp cell culture miniplates. The cells were then permeabilized using XF plasma membrane permeabilizer (Cat. No. 102504, Agilent Technologies) and supplemented with 4 mmol/L of ADP plus vehicle control (0.03% DMSO) or ceritinib (1.5 μmol/L). The OCR was then measured using a Seahorse XFp extracellular flux analyzer, as described previously (16), after the addition of 10 mmol/L glutamate and 10 mmol/L malate (to measure complex I-linked respiration), 10 mmol/L succinate in the presence of 2 μmol/L complex I inhibitor rotenone (to measure complex II/III-linked respiration) and 10 mmol/L ascorbate + 100 μmol/L TMPD in presence of 2 μmol/L antimycin A (to measure complex IV–linked respiration).

Complex V activity assay

Complex V activity was measured in OVCAR-8 whole-cell extracts with an ATP synthase enzyme activity microplate assay kit (ab109714, Abcam). Cells were treated with vehicle control (DMSO), ceritinib (1.5 μmol/L), or oligomycin (100 nmol/L, positive control) for 12 hours. The cells were then harvested, washed once with ice-cold PBS, and lysed by three freeze-thaw cycles. Proteins were detergent extracted and loaded at 50 μg/50 μL in triplicates into the wells of a microplate precoated with monoclonal anti-ATP synthase antibody. A 40-μL aliquot of lipid mix was added to each well after incubation for 3 hours at room temperature. Plates were then incubated for 45 minutes at room temperature, and 200 μL of reagent mix was added. The ATP synthase activity rate was measured spectrophotometrically as the change in absorbance at 340 nm over 90 minutes and expressed as changes of absorbance per minute per 50 μg protein as described by the supplier.

ATP assay

Two million OVCAR-8 or COV362 cells were plated onto 10-cm tissue culture dishes, allowed to grow overnight, and treated with vehicle or ceritinib for 12 hours. Total ATP levels in the cells were then measured using a method that detects ATP-dependent generation of glycerol phosphate, followed by colorimetric detection (catalog no. ab83355, Abcam).

ROS assay

One million OVCAR-8 or COV362 cells were plated onto 10-cm tissue culture dishes, incubated overnight, and treated with vehicle or

indicated concentrations of ceritinib, olaparib, or ceritinib + olaparib for 12–18 hours. ROS and peroxide levels were measured using a cell-based fluorogenic assay kit (catalog no. ab139476, Abcam).

Quantitative real-time PCR

Total RNA was extracted from cells using an miRNeasy mini kit (catalog no. 217004, Qiagen) following the supplier's instructions. cDNA was synthesized from 1 μg of total RNA using oligo(dT) primers and SuperScript III reverse transcriptase (catalog no. 18080–044, Thermo Fisher Scientific), and qRT-PCR was performed using iTaq Universal SYBR Green Supermix (catalog no. 1725120, Bio-Rad) on a CFX96 real-time PCR system (Bio-Rad) using 25 ng cDNA template. GAPDH was used as an internal control to normalize mRNA expression. All qPCR primers were purchased from Integrated DNA Technologies (IDT) and are listed in Supplementary Table S1.

PARP trapping assay

The PARP trapping assays were performed as previously described (17). To prepare nuclear soluble and chromatin-bound fractions of PARP1, we used a Subcellular Protein Fractionation Kit from Thermo Fisher Scientific (catalog no. 78840), following the supplier's instructions.

Western blotting

Cells were lysed in ice-cold cell lysis buffer (50 mmol/L HEPES, 1% Triton X-100, 10 mmol/L NaF, 30 mmol/L $Na_4P_2O_7$, 150 mmol/L NaCl, and 1 mmol/L EDTA freshly supplemented with 10 mmol/L β-glycerophosphate, 1 mmol/L Na_3VO_4, 20 μg/mL pepstatin A, 10 μg/mL aprotinin, 20 μg/mL leupeptin, 40 μmol/L microcystin-LR). Immunoblotting was done using the following primary antibodies: mouse monoclonal RAD51C (1:1,000, catalog no. NB100–177, Novus Biologicals, RRID:AB_10001856), rabbit monoclonal XRCC1 (1:1,000, catalog no. 3631-1, Epitomics, RRID: AB_10897570), rabbit monoclonal IRS1 (1:1,000, catalog no. 3407T, Cell Signaling Technology, RRID:AB_2127860), rabbit polyclonal phospho-IRS1 (Tyr612; 1:1,000, catalog no. 44-816G, Thermo Fisher Scientific, RRID:AB_2533768), rabbit monoclonal PARP1 (1:1,000, catalog no. ab32138, Abcam, RRID:AB_777101), rabbit monoclonal histone H3 (1:1,000, catalog no. 4499, Cell Signaling Technology, RRID:AB_10544537), and mouse monoclonal HSP90 (D. Toft, Mayo Clinic, H9010). Secondary antibodies used were horseradish peroxidase–conjugated anti-mouse immunoglobulin G (1:10,000, catalog no. 7076S, Cell Signaling Technology, RRID: AB_330924) and anti-rabbit immunoglobulin G (1:10,000, catalog no. 7074S, Cell Signaling Technology, RRID:AB_2099233).

Indirect immunofluorescence

For immunostaining of 8-oxo-dG in OVCAR-8 and COV362 cells, the cells were plated (4,000 cells per well) on 8-well Nunc Lab-Tek II Chamber Slide System slides (catalog no. 154534, Thermo Fisher Scientific), cultured overnight, and treated with vehicle or ceritinib. After 48 hours, the cells were fixed with ice-cold methanol:acetone (7:3) for 7 minutes at −20°C, washed once with PBS, and incubated with RNase A (200 μg/mL) in PBS for 1 hour at 37°C. After cells were washed twice with PBS, DNA was denatured by incubation in 70 mmol/L NaOH, 0.14 mol/L NaCl, and 40% methanol for 5 minutes on ice. The denaturing solution was removed by aspiration, and cells were then incubated with proteinase K (5 μg/mL in 20 mmol/L Tris HCl, pH 7.4, and 2 mmol/L $CaCl_2$) for 10 minutes at 37°C. Nonspecific antibody binding was blocked with 5% bovine serum albumin in 0.2% Triton X-100 in PBS for 30 minutes, and cells were incubated overnight with antibody to 8-oxo-dG (mouse monoclonal, 1:250, catalog no. 4354-MC-050, Trevigen, RRID:AB_1857195). Cells were washed three times with PBS and incubated with anti-mouse Alexa Fluor 488–conjugated secondary antibody (1:500; Thermo Fisher Scientific) for 1 hour in the dark, then washed once with PBS, incubated with Hoechst-33342 (1:1,000, catalog no. 62249, Thermo Fisher Scientific) for 2 minutes to stain DNA, mounted in Prolong Gold Antifade (Thermo Fisher Scientific), and images were captured with a Zeiss LSM780 confocal microscope equipped with ×40 or ×100 objective. For immunostaining of γH2AX and PARP, cells were fixed with 3% paraformaldehyde in PBS for 15 minutes at room temperature, blocked with 5% BSA in 0.2% Triton X-100 in PBS for 30 minutes, incubated overnight with antibodies to γH2AX (mouse monoclonal, 1:350, catalog no. 05–636, Millipore, RRID:AB_309864) and PARP (mouse monoclonal, 1:350, catalog no. 4335-MC-100, Trevigen, RRID: AB_2572318), and processed for confocal microscopy as described above.

For immunostaining of 8-oxo-dG in PDX specimens, formalin fixed, paraffin-embedded PDX tumor tissues were sectioned into approximately 4-μm slices onto glass slides. The tissue sections were then de-paraffinized in xylene for 10 minutes, sequentially rehydrated in 100%, 90%, and 70% ethanol solutions for 1 minute each, washed twice in PBS, and permeabilized with 0.2% Triton X-100 in PBS for 10 minutes at room temperature. After washing twice in PBS, tissue sections were incubated with 10 μg/mL proteinase K in PBS for 30 minutes at 37°C and then incubated with 100 μg/mL RNase A in 10 mmol/L Tris-HCl, pH 7.4, 1 mmol/L EDTA, and 0.4 mmol/L NaCl for 1 hour at 37°C. The DNA was then denatured by soaking the slides in 4 N HCl for 10 minutes at room temperature. After neutralizing the samples with 50 mmol/L Tris base for 5 minutes at room temperature, the nonspecific binding sites were blocked with 10% goat serum in PBS for 30 minutes at room temperature, and the sections were incubated with the above-mentioned mouse monoclonal 8-oxo-dG antibody (diluted at 1:600 in 10% goat serum) overnight at 4°C. The sections were washed three times in PBS, incubated with anti-mouse Alexa Fluor 488–conjugated secondary antibody (1:600; Thermo Fisher Scientific) for 1 hour in the dark, then washed once with PBS, incubated with Hoechst-33342 (1:1,000, catalog no. 62249, Thermo Fisher Scientific) for 2 minutes to stain DNA, and processed for confocal microscopy as described above.

HR assay

HR assays were performed using OVCAR-8-DR-GFP cells (14). The cells were treated with vehicle or ceritinib for 72 hours and GFP fluorescence was analyzed via flow cytometry as described previously (14).

PDX studies

Fresh human tumor tissues from consenting patients with ovarian cancer were collected at the time of primary debulking surgery and coded with a patient heterotransplant (PH) number in accordance with the Mayo Clinic Institutional Review Board and the Health Insurance Portability and Accountability Act regulations. A guarantee that all human subject research at Mayo has been reviewed by the IRB has been given to the U.S. Department of Health and Human Services in a Federal-wide Assurance (FWA00005001) and is guided by the statement of principles outlined in The Belmont Report. An IRB-approved written informed consent form was documented in the electronic medical record of every patient. All animal procedures were approved by the Mayo Clinic Institutional Animal Care and Use Committee, consistent with all policies of the American Veterinary

Medical Association. Tumors were established by intraperitoneal injection into female SCID beige mice (C.B.-17/IcrHsd-*Prkdcscid Lystbg*; ENVIGO) as previously described (18). Briefly, approximately 0.3 mL of minced patient tumor was mixed 1:1 with McCoy's 5a medium containing rituximab (10 mg/kg, Genentech, Inc.) to prevent lymphoma development (19). Mice were monitored for engraftment and PDX tumors were expanded into additional mice when the tumor dimension was assessed as greater than or equal to 10% of body weight or if humane endpoints were met (humane endpoints: weight loss greater than or equal to 20% of body weight, inability to ambulate, inability to reach for food and/or water, tumors that have ulcerated, or a body condition score of 5 or less using the IACUC approved scoring system). PDX tumors were cryogenically preserved for future experiments (18). The minimal information standard for PDX models is provided in Supplementary Table S2.

For *in vivo* PDX drug studies, expanded PDX tumors were minced and injected into the peritoneal space of SCID Beige as described above for initial tumor inoculations. When tumors reached a minimum threshold of 0.3–0.5 cm^2 cross-sectional area by ultrasound, animals were randomized and used for drug studies. For single-agent ceritinib studies, mice bearing tumors received saline control or ceritinib 100 mg/kg by daily oral gavage for 28 days. For ceritinib + olaparib combination studies, mice received saline control, ceritinib (100 mg/kg), olaparib (50 mg/kg), or ceritinib + olaparib (100 mg/kg + 50 mg/kg) by daily oral gavage for up to 9 weeks. Mice were removed from the study if tumor dimensions determined by ultrasound indicated that tumors were greater than or equal to 10% of body weight or if humane endpoints (described above) were met. Ultrasound measurements were taken weekly.

PDX growth curves were analyzed by repeated measures analysis implemented via linear mixed effects models (20). The dependent variable was ultrasound tumor area on the natural log scale. Independent variables were day, treatment arm, and the day by treatment interaction, where the day variable was centered. The functional form of the mean model was chosen based on Akaike information criterion (AIC), Bayesian information criterion (BIC), plots of predicted trajectories and residual plots assuming independent observations. Additional polynomial terms were added to the mean model in a hierarchical manner as required to describe the growth trajectories as follows: A quadratic day term was added for PH048, PH115, and PH475; cubic day term for PH039 and PH345; cubic day by treatment term for PH038. The form of the mean model was then held fixed and plausible covariance structures estimated via restricted maximum likelihood estimation; AIC and BIC indicated that a spatial (power) covariance structure was a good fit for all PDX models. Treatment arms were compared via multiple degree of freedom coincident curve hypothesis tests. Analyses were performed via R (21) and SAS software (copyright 2016, SAS Institute Inc.).

Results

Ceritinib lacks single-agent activity in *ALK*-altered ovarian cancer PDXs

Analyses of genomic and transcriptomic profiles of ovarian cancer PDX tumors, as well as examination of The Cancer Genome Atlas database, showed that a subset of HGSOCs have *ALK* gene alterations that include *ALK* amplification, *ALK* rearrangement, and an *ALK* mutation of unknown significance in the kinase domain, as well as high levels of *ALK* mRNA (Supplementary Fig. S1A and S1B). Given that *ALK* rearrangements and mutations drive the proliferation of a subset of NSCLCs, we explored whether ceritinib, an ALK inhibitor, had activity in ovarian cancer PDX models that harbor *ALK* alterations. Despite these *ALK* alterations, ceritinib had limited activity in the PDX models with amplified, rearranged, mutated, or highly expressed *ALK* (Supplementary Figs. S2 and S3; Supplementary Table S3).

Ceritinib synergizes with PARPis in HR-proficient and -deficient ovarian cancer cells

In parallel studies, we also assessed the effect of combining ceritinib with PARPis. These studies demonstrated that ceritinib synergized with the PARPi olaparib in HR-proficient OVCAR-8 cells (**Fig. 1A** and **B**), although ceritinib did not affect cisplatin cytotoxicity (Supplementary Fig. S4A). Similar results were seen with the PARPi veliparib (**Fig. 1C**). Ceritinib also synergized with olaparib in COV362 cells (**Fig. 1D** and **E**), which have a deleterious *BRCA1* mutation (22), and in OVCAR-8 cells that were depleted of RAD51C (**Fig. 1F**; Supplementary Fig. S4B), a key component of the HR pathway that is mutated or methylated in a subset of HGSOCs (2, 3). Additional studies showed that ceritinib synergized with olaparib in HR-proficient prostate cancer PC3 cells but not in breast cancer MDA-MB-231 cells (Supplementary Fig. S4C and S4D). These results demonstrate that ceritinib synergizes with PARPis, but not cisplatin, in HR-proficient and -deficient HGSOC cell lines and possibly in certain other cancers that are treated with PARPis.

Ceritinib + PARPi synergy is not associated with disruption of HR or inhibition of known kinase targets of ceritinib

Defects in HR sensitize cells to PARPis (3), suggesting a potential mechanism for the synergy of ceritinib + olaparib. However, consistent with the observation that ceritinib did not synergize with cisplatin (Supplementary Fig. S4A), which induces lesions repaired by HR (3), ceritinib did not inhibit HR in the DR-GFP HR reporter assay (Supplementary Fig. S5A; ref. 23).

We next assessed whether ceritinib synergized with PARPis by inhibiting ALK or other known targets of ceritinib, including IGF1R, FAK1, FES, ROS1, CAMKK2, EGFR, RSK1, and RSK2 (24). *ALK* mRNA was not detectable in OVCAR-8 cells compared with PC3 cells (Supplementary Fig. S5B), which express low levels of ALK (25, 26). In addition, siRNA-mediated depletion of ALK did not sensitize the cells to PARPis (Supplementary Fig. S5C). Finally, disabling the other known kinase targets of ceritinib using siRNAs or small-molecule inhibitors did not sensitize OVCAR-8 cells to PARPis (Supplementary Fig. S5D–S5J). Together, these findings suggest that ceritinib synergizes with PARPis via a mechanism independent of its ability to inhibit ALK or other kinases known to be targeted by ceritinib.

Ceritinib inhibits oxygen consumption, induces ROS production, and causes DNA damage that is repaired by BER

Several considerations prompted us to test the hypothesis that ceritinib sensitizes to PARPis by enhancing the production of ROS, which then induce DNA damage that is repaired in a PARP-dependent manner. First, a previous study showed that high concentrations of ceritinib inhibited mitochondrial respiration of purified rat liver mitochondria (27), raising the possibility that ceritinib might do the same thing in intact cells. Second, inhibition of mitochondrial respiration elevates levels of ROS (28–30), which induce DNA lesions that are known to be repaired by PARP-dependent repair processes, primarily BER (5).

In support of the idea that ceritinib affects mitochondrial respiration, we found that ceritinib suppressed the OCR, a readout for mitochondrial respiration, in intact OVCAR-8 and COV362 cells (**Fig. 2A** and **B**). Additional analyses showed that in detergent-permeabilized cells

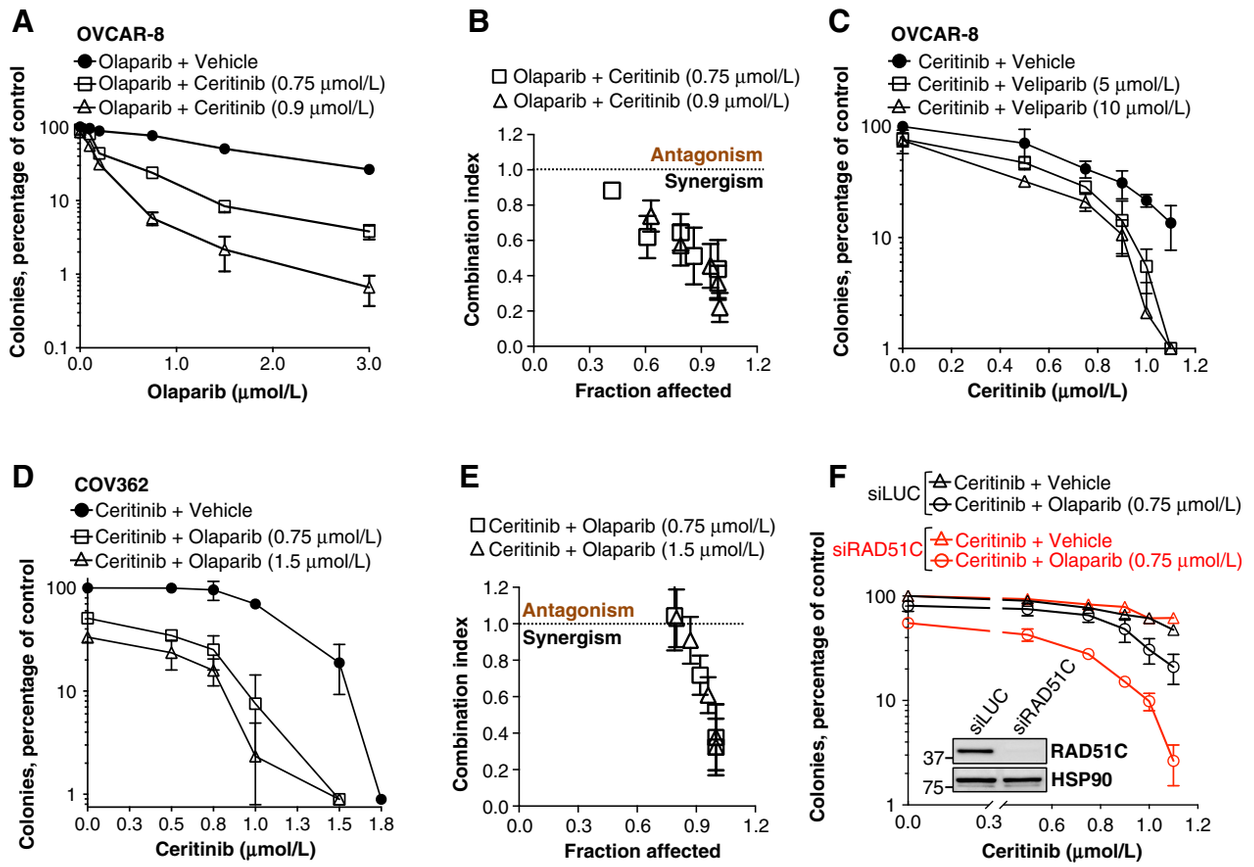

Figure 1.

Ceritinib synergizes with PARPis in HR-proficient and -deficient ovarian cancer cells. **A–E,** OVCAR-8 (**A–C**) or COV362 (**D** and **E**) cells were plated as single cells and cultured in the continued presence of indicated concentrations of ceritinib and olaparib (**A**, **B**, **D**, and **E**) or veliparib (**C**) for 8–10 days to form colonies. Colonies were stained with Coomassie Blue and those with >50 cells/colony were counted manually. Graphs (**A**, **C**, and **D**) are representative of three independent experiments. Error bars, means ± SD of three technical replicates in the representative experiment. Combination index (CI) values (**B** and **E**) were calculated using the Chou–Talalay method in CalcuSyn software. CI > 1, CI = 1, and CI < 1 are antagonistic, additive, and synergistic, respectively. CI values (**B** and **E**) show the mean ± SEM for the three independent experiments. **F,** OVCAR-8 cells were transfected with control luciferase (siLUC) or a RAD51C siRNA pool. Forty-eight hours later, the cells were harvested, immunoblotted for RAD51C and HSP90 (loading control), and subjected to colony formation assays as in **A**, **C**, and **D**. Graph is representative of three independent experiments. Error bars, means ± SD of three technical replicates in the representative experiment.

ceritinib selectively inhibited complex I of the electron transport chain (**Fig. 2C** and **D**), an emerging target for cancer therapy (31). Importantly, OCR inhibition was not observed in a panel of other ALK inhibitors (Supplementary Fig. S6A) and was seen at ceritinib concentrations that occur at steady state in the plasma of patients treated with this agent (32). In agreement with its effect on mitochondrial respiration, ceritinib also reduced ATP levels (**Fig. 2E** and **F**) without inhibiting glycolysis (Supplementary Fig. S6B), and it increased ROS levels, including peroxide levels, in both OVCAR-8 and COV362 cells (**Fig. 2G** and **H**).

To determine whether ceritinib-induced ROS cause DNA damage, OVCAR-8 and COV362 cells were treated with ceritinib and H_2O_2 (as a positive control). Ceritinib, like H_2O_2, induced accumulation of (i) 8-oxo-dG (**Fig. 3A** and **B**), a lesion produced by OH attack; (ii) γH2AX (**Fig. 3C**), a marker of DNA damage and replication stress (33, 34); and (iii) poly(ADP-ribose) polymers (**Fig. 3D**), which are formed at DNA damage sites by active PARP (35–39). Together, these results demonstrate that ceritinib induces ROS accumulation and causes DNA damage that activates PARP.

We next asked whether ceritinib-induced DNA damage contributed to cytotoxicity. First, we inhibited ATR, a DNA damage-activated checkpoint kinase that protects cells from genotoxic stress (40). These studies showed that ATR inhibition with berzosertib (VE-822; ref. 41) sensitized cells to ceritinib (**Fig. 3E**). Second, because (i) PARP plays a key role in BER and (ii) ROS cause damage repaired by BER, we examined the role of the BER pathway in ceritinib cytotoxicity by depleting XRCC1, a key member of the BER pathway that is recruited by activated PARP to sites of damage (5). As shown in **Fig. 3F** and **G**, XRCC1 depletion sensitized cells to ceritinib.

Finally, we examined several other aspects of the role of ROS in the synergy between ceritinib and PARPis. First, we examined how combining ceritinib with olaparib affected OCR, ROS accumulation, and oxidative DNA damage. Consistent with previous findings with PARPis in ovarian cancer cells (42, 43), olaparib alone increased ROS and 8-oxo-dG levels (**Fig. 4A–C**) but had minimal impact on OCR (Supplementary Fig. S6C). In cells exposed to ceritinib + olaparib, ROS and 8-oxo-dG levels were somewhat further increased (**Fig. 4A–C**), and

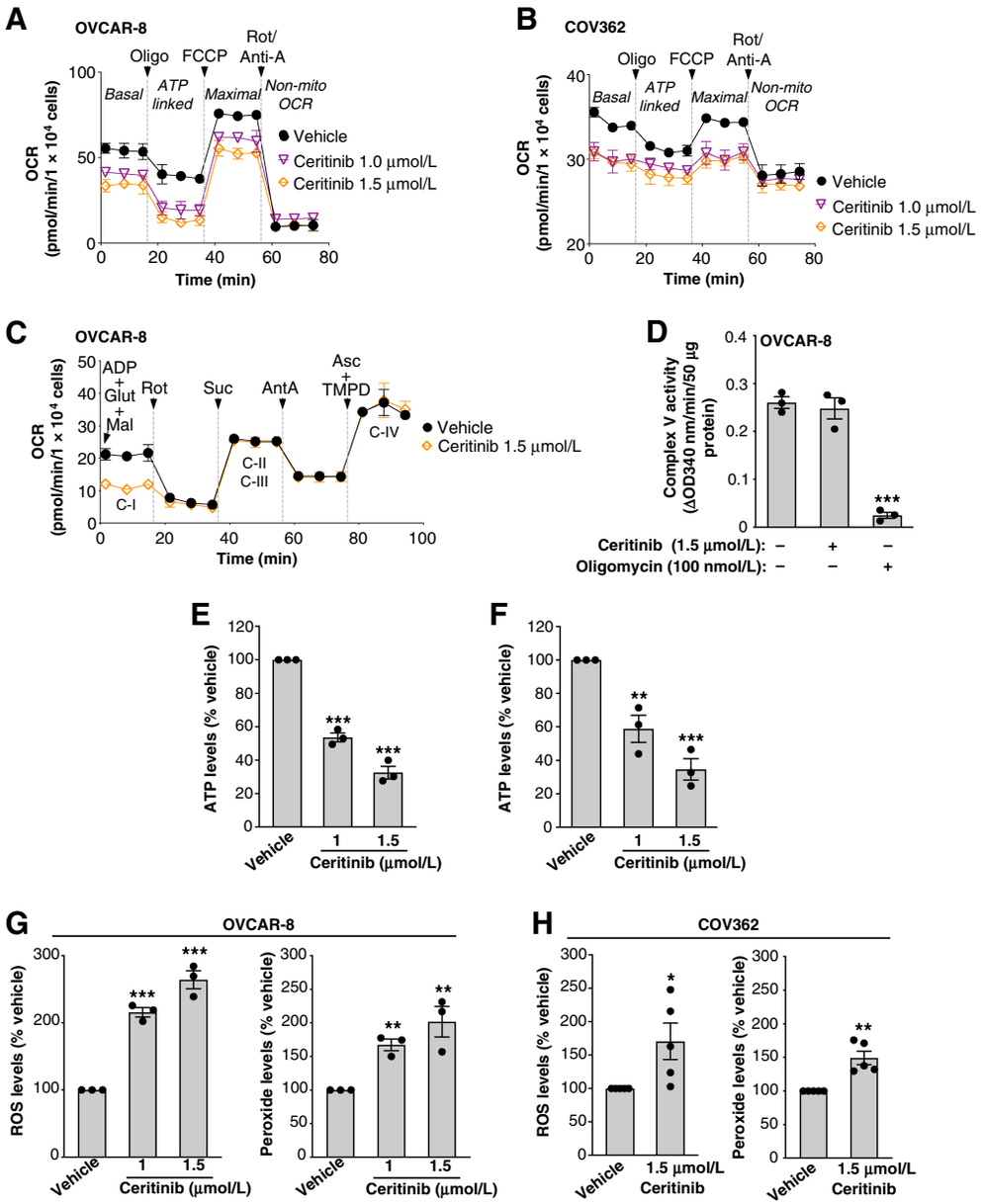

Figure 2.

Ceritinib inhibits OCR, reduces ATP levels, and induces ROS. **A** and **B,** OVCAR-8 (**A**) or COV362 (**B**) cells were treated with vehicle (0.03% DMSO) or ceritinib for 12 hours, and OCRs were measured under basal conditions as well as after the sequential additions of oligomycin (Oligo), an inhibitor of ATP synthase; FCCP, an uncoupler of mitochondrial oxidative phosphorylation; and rotenone and antimycin A (Rot/Anti A), two inhibitors of mitochondrial electron transport complexes I and II, respectively, using a Seahorse XFp extracellular flux analyzer. Data are representative of three independent experiments. Error bars, means ± SEM of two technical replicates in the representative experiment. **C,** OVCAR-8 cells were permeabilized using the XF plasma membrane permeabilizer and supplemented with 4 mmol/L of ADP plus vehicle control (0.03% DMSO) or ceritinib (1.5 μmol/L) and the OCR was then measured using a Seahorse XFp extracellular flux analyzer after sequential addition of 10 mmol/L glutamate + 10 mmol/L malate (to measure complex I–linked respiration), 2 μmol/L rotenone (to inhibit complex I), 10 mmol/L succinate (to measure complex II/III–linked respiration), 2 μmol/L antimycin A (to inhibit complex III), and 10 mmol/L ascorbate + 100 μmol/L TMPD (to measure complex IV–linked respiration). Data are representative of three independent experiments. Error bars, means ± SEM of three technical replicates in the representative experiment. **D,** OVCAR-8 cells were treated with vehicle control (0.03% DMSO), ceritinib (1.5 μmol/L), or oligomycin (100 nmol/L; positive control) for 12 hours. The cells were then harvested, proteins were detergent extracted, and complex V activity was measured spectrophotometrically in triplicate with an ATP synthase enzyme activity microplate assay kit and expressed as changes of absorbance per minute per 50 μg protein. The data are mean ± SEM for three independent experiments. ***, $P < 0.001$ relative to vehicle control, unpaired Student *t* test. **E** and **F,** OVCAR-8 (**E**) or COV362 (**F**) cells were treated with vehicle or ceritinib for 12 hours, and ATP levels were measured and normalized to vehicle. Data are means ± SEM of three independent experiments. **, $P < 0.01$; ***, $P < 0.001$ relative to vehicle control, unpaired Student *t* test. **G** and **H,** OVCAR-8 (**G**) or COV362 (**H**) cells were treated with vehicle or ceritinib for 12 and 18 hours, respectively, and ROS (left; **G** and **H**) and peroxide (right; **G** and **H**) levels were measured and normalized to vehicle. Data are means ± SEM of three independent experiments for OVCAR-8 and five independent experiments for COV362 cells. *, $P < 0.05$; **, $P < 0.01$; ***, $P < 0.001$, relative to vehicle control, unpaired Student *t* test.

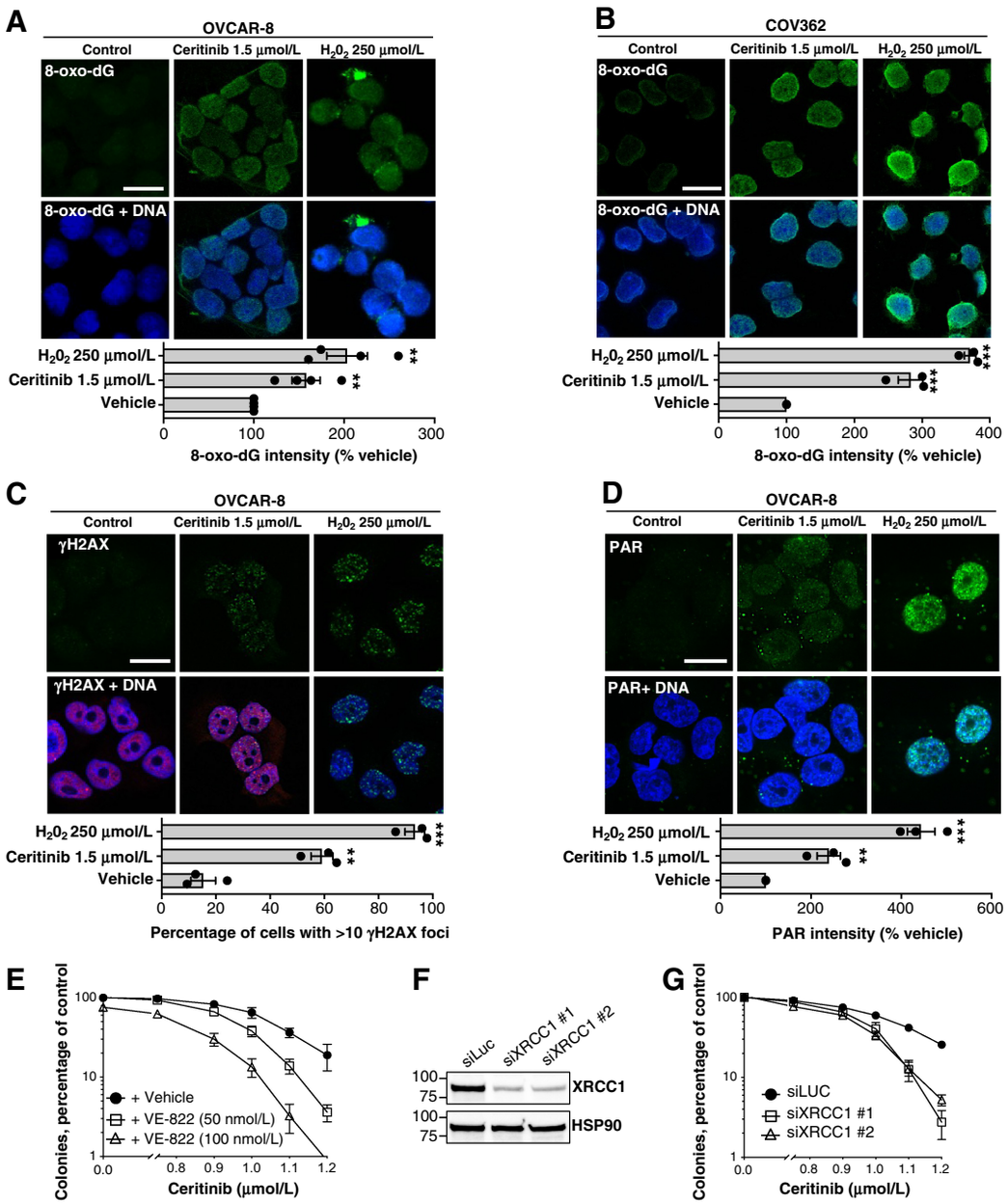

Figure 3.

Ceritinib induces oxidative DNA damage that is repaired via BER. **A–D,** OVCAR-8 (**A**, **C**, and **D**) or COV362 (**B**) cells were treated with vehicle (0.03% DMSO) or ceritinib for 48 hours or H_2O_2 for 15 minutes (positive control) and immunostained (green) for 8-oxo-dG (**A** and **B**), γH2AX (**C**), or poly(ADP-ribose) polymers (PAR), and counterstained for DNA (blue; **D**). All images are representative of four (**A**) or three (**B–D**) independent experiments. Quantification of fluorescence intensity (**A**, **B**, and **D**) of >100 cells/treatment was performed using ImageJ software (NIH). Values were normalized to vehicle control and are shown below respective image. γH2AX foci (**C**) were counted in >50 cells/treatment. All graphs show mean ±SEM, $n = 3$ or 4 independent experiments. **, $P < 0.01$; ***, $P < 0.001$ relative to vehicle control, unpaired Student t test; scale bars, 20 μm. **E,** OVCAR-8 cells were plated as single cells and treated with indicated concentrations of ceritinib and VE-822 for 8 days. Colonies were stained with Coomassie Blue and those with >50 cells/colony were counted manually. Graphs are representative of three independent experiments. Error bars, means ± SD of three technical replicates in the representative experiment. **F** and **G,** OVCAR-8 cells were transfected with control luciferase (siLUC) or two different XRCC1 siRNAs. Forty-eight hours later, the cells were harvested, immunoblotted for XRCC1 and HSP90 (loading control; **F**), and subjected to colony formation assay (**G**). Graph is representative of three independent experiments. Error bars, means ± SD of three technical replicates in the representative experiment.

PARP trapping on chromatin was increased (**Fig. 4D**), indicating that the drug combination created additional ROS-induced DNA damage compared with either agent alone. Second, we found that IACS-010759, an inhibitor of complex I of the mitochondrial electron transport chain that increases ROS levels and has shown preclinical activity (44–48), also synergized with olaparib (Supplementary Fig. S6D). Third, we found that the antiproliferative effects of ceritinib + olaparib were blunted by the addition of the

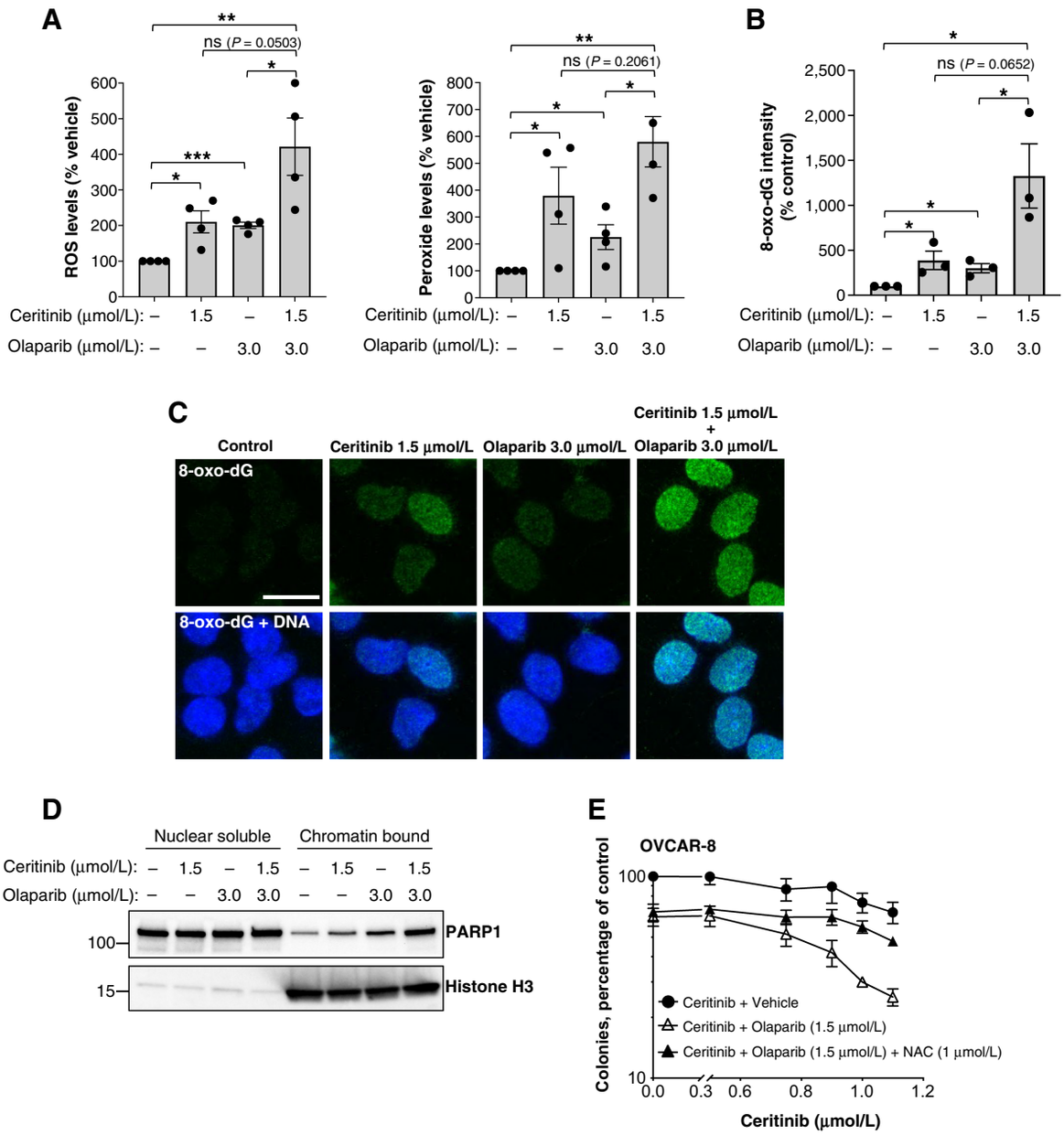

Figure 4.

Ceritinib + olaparib further augment ROS levels and oxidative DNA damage. **A,** OVCAR-8 cells were treated with vehicle (0.03% DMSO) or indicated concentrations of ceritinib, olaparib, or ceritinib + olaparib for 12 hours, and ROS (left) and peroxide (right) levels were measured and normalized to vehicle. Data are means ± SEM of four independent experiments. *, $P < 0.05$; **, $P < 0.01$; ***, $P < 0.001$ relative to vehicle control, unpaired Student *t* test. **B** and **C,** OVCAR-8 cells were treated with vehicle (0.03% DMSO), ceritinib, olaparib, or ceritinib + olaparib for 48 hours and immunostained for 8-oxo-dG (green) and counterstained for DNA (blue). All images in **C** are representative of three independent experiments; scale bars, 20 μm. Quantification of fluorescence intensity (**B**) of 100 cells/treatment was performed using ImageJ software (NIH). Values were normalized to vehicle control. Data in **C** are mean ± SEM; $n = 3$ independent experiments. *, $P < 0.05$ relative to vehicle control, unpaired Student *t* test; ns, not significant. **D,** OVCAR-8 cells were treated with vehicle, ceritinib, olaparib, or ceritinib + olaparib for 24 hours, and nuclear soluble and chromatin bound fractions of PARP1 were analyzed by Western blotting. Histone H3 was used as positive marker for chromatin bound fraction. **E,** OVCAR-8 cells were plated as single cells and cultured in the continued presence of indicated concentrations of ceritinib and olaparib ± N-acetylcysteine (NAC) for 8–10 days to form colonies. Colonies were stained with Coomassie Blue and those with >50 cells/colony were counted manually. Graph is representative of three independent experiments. Error bars, means ± SD of three technical replicates in the representative experiment.

antioxidant N-acetylcysteine (**Fig. 4E**), thus, indicating that ROS contributes to cytotoxicity of the combination.

Taken together, these results support a model in which ceritinib synergizes with PARPis, by inhibiting mitochondrial respiration, leading to increased ROS-induced DNA damage that is repaired by the PARP-dependent BER pathway and possibly other DNA repair pathways.

The ceritinib + PARPi combination has activity in HGSOC PDX models *in vivo*

The cell line findings (**Fig. 1A**, **B**, and **D–F**) raised the prospect that a ceritinib + olaparib combination might have activity in HGSOC. To assess this possibility, we examined the activity of ceritinib, olaparib, and the combination in HGSOC PDX mouse models *in vivo* using doses of olaparib (50 mg/kg/d) and ceritinib (100 mg/kg/d) that previously exhibited antitumor activity in mice bearing ovarian or lung tumors as monotherapy, respectively (49, 50). When these agents were combined at the maximum tolerated single-agent doses, ceritinib + olaparib was well tolerated, as demonstrated by limited weight loss (Supplementary Fig. S7A), no evidence of myelosuppression (Supplementary Fig. S7B), and limited elevations of total bilirubin and alkaline phosphatase (Supplementary Fig. S7B).

We then applied this treatment to a series of HGSOC PDX models with differing HR gene alterations and HRD scores (high HRD scores are correlated with HR defects). In agreement with the increased activity of ceritinib + olaparib in RAD51C-depleted OVCAR-8 cells (**Fig. 1F**; Supplementary Fig. S4B), this combination caused statistically significantly greater tumor regression than either agent alone in three olaparib-responsive PDX models with probable HR deficiencies (*RAD51C*-mutant PH345; HRD-high PH038; *RAD51C*-methylated PH039; **Fig. 5A–C**; Supplementary Fig. S8A, and Supplementary Table S3). Moreover, in the PH038 and PH039 models, no tumor was detectable in 7/8 and 11/14 mice, respectively, at 9 weeks, a finding that did not occur with either agent alone. In PDX models PH115 and PH048, with no known HR defects (i.e., low HRD scores and no mutations in HR genes), ceritinib + olaparib had limited activity despite being statistically significantly different from the vehicle-treated control for PH115 (**Fig. 5D** and **E**; Supplementary Fig. S8A; Supplementary Table S3).

On the basis of our observations that ceritinib induced oxidative stress and DNA damage in ovarian cancer cell lines, we next asked whether ceritinib also induced these events in PDX models. As a marker for oxidative stress and DNA damage, we assessed 8-oxo-dG levels in PH345 and PH039, two models that robustly responded to ceritinib + olaparib, at the end of the 21- or 28-day treatment. Because there was insufficient (or no) tumor found in the mice treated with ceritinib + olaparib, we focused our analyses on the ceritinib-treated tumors. As shown in **Fig. 6**, ceritinib induced 8-oxo-dG in the PDX tumors compared with vehicle-treated control tumors. Similarly, in a PDX tumor model in which tumors from ceritinib + olaparib were present during treatment, we observed increased 8-oxo-dG levels in tumors treated with ceritinib or olaparib alone, as well as greater oxidative stress in the tumors treated with ceritinib + olaparib (Supplementary Fig. S8B).

Collectively, these observations show that (i) ceritinib induced oxidative DNA damage in PDX tumors *in vivo*, (ii) ceritinib + olaparib enhanced tumor regression or inhibited growth even in tumors in which olaparib had reduced activity (e.g., PH115), and (iii) the combination had even greater activity in PARPi-responsive tumors.

Discussion

Here, we examined the activity of ceritinib, both as monotherapy and with PARPis, in preclinical models of HGSOC. Results of these studies indicate that ceritinib lacks monotherapy activity but nonetheless enhances the activity of PARPis in HGSOC models without substantial toxicity, a result that has potentially important clinical implications.

To assess the activity of ceritinib monotherapy, we used PDXs with high levels of ALK mRNA as well as PDXs with *ALK* alterations, including *ALK* amplification, an *ALK* kinase domain mutation of unknown significance, and an *ALK* gene fusion. Ceritinib was not active in HGSOC PDXs with these alterations (Supplementary Figs. S2 and S3), suggesting that ALK is not driving the proliferation of the HGSOC models tested. One limitation of our study is that we did not systematically address whether ALK mRNA expression levels or *ALK* alterations impact responses to the combination of ceritinib + PARPis. However, as shown for PH048, which has an *ALK* translocation, ceritinib + olaparib did not cause tumor regression. Although we cannot rule out that ALK inhibition could affect the activity of ceritinib + olaparib in some HGSOC tumors, this seems unlikely given that our studies show that ceritinib is operating by an ALK-independent mechanism in ovarian cancer cells.

PARPis are currently used as monotherapy to treat HGSOC with and without *BRCA1*/2 mutations in the frontline and recurrent settings as maintenance therapy and in recurrent disease in place of chemotherapy (6, 7). The antineoplastic activity of PARPi monotherapy in these settings reflects, at least in part, the ability of PARPis to inhibit poly(ADP-ribosyl)ation, which results in PARP trapping at sites of DNA damage, disruption of repair, and collapse of replication forks that cannot be efficiently resolved in HR-deficient cells, ultimately leading to cell death (3, 6, 7). Despite the success of PARPis in extending progression-free survival (PFS), disease relapse remains common. Accordingly, there is substantial interest in identifying agents that can be combined with PARPis to make PARPi-resistant tumor sensitive to PARPis and/or to extend PFS and overall survival (OS) in PARPi-sensitive tumors.

Previous preclinical studies have demonstrated that inhibiting a variety of different tyrosine kinase receptors or their downstream transducers can sensitize tumor cells to PARPis by reducing expression of BRCA1, BRCA2, RAD51, and other HR components, thereby disrupting HR repair (51–53). Indeed, these findings have been translated into the clinic. For example, the anti-angiogenic agent cediranib, which inhibits VEGF receptor tyrosine kinase activity, downregulates the expression of BRCA1, BRCA2, and RAD51 by inducing hypoxia and by inhibiting PDGF receptors in tumor cells, thereby blocking a signaling pathway that leads to transcription of BRCA1, BRCA2, and RAD51 (53). Consistent with these preclinical findings, a phase 2 trial of cediranib + olaparib in relapsed platinum-sensitive HGSOC demonstrated increased PFS and OS compared with olaparib alone, with the survival benefit primarily in patients with wild-type *BRCA1/2* tumors (54). Taken together, these findings indicate that blocking receptor tyrosine kinase signaling may be a useful way to disrupt HR and increase the activity of PARPis in the clinic.

In contrast, the results presented here identify a novel mechanism by which the kinase inhibitor ceritinib can synergize with PARPis. Ceritinib does not inhibit HR, which explains why it does not synergize with cisplatin, an agent that induces DNA damage that is repaired, in part, by HR (3). Instead, ceritinib disrupted mitochondrial respiration by inhibiting complex I of the electron transport chain, an event that is

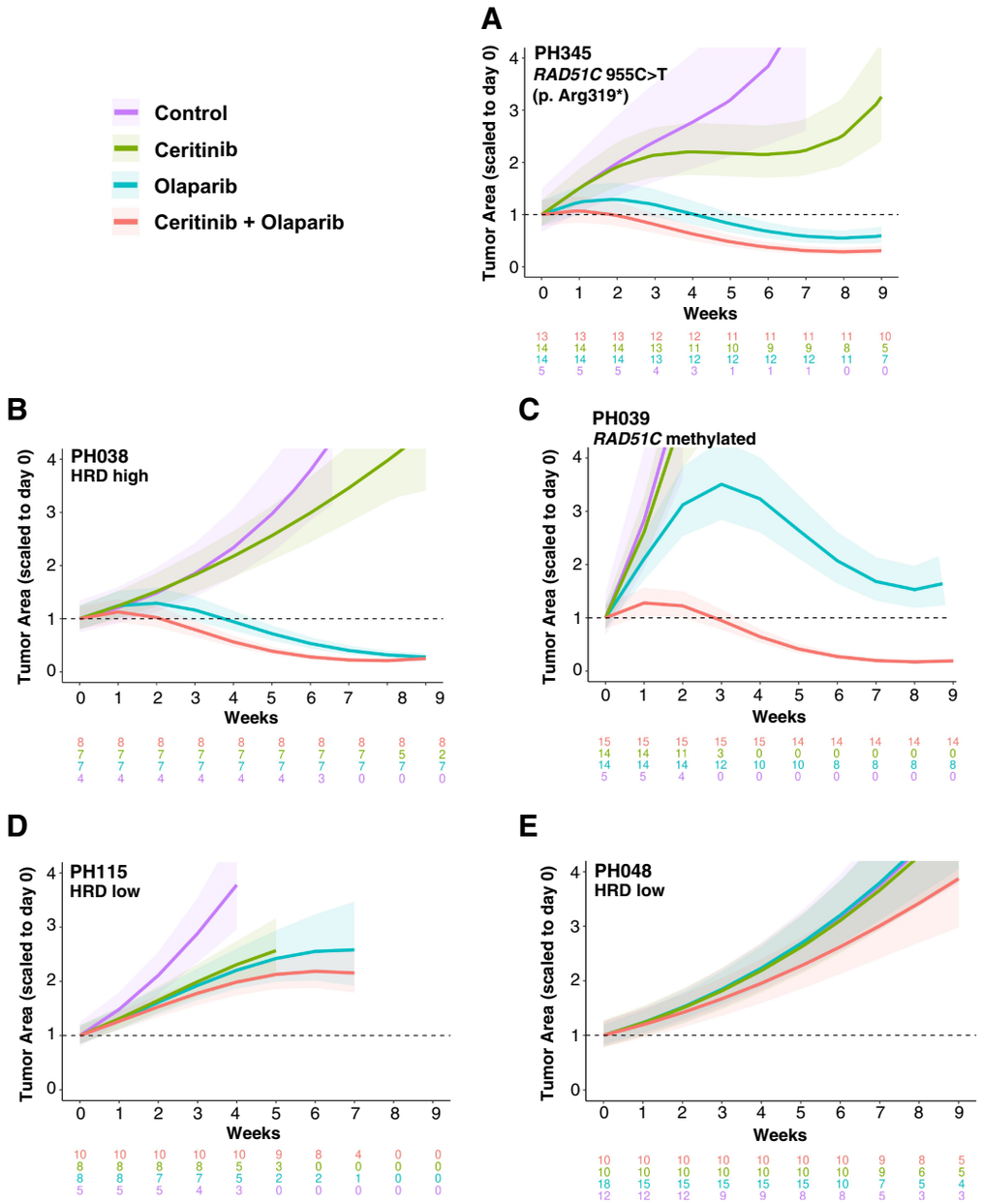

Figure 5.

Combination effects of ceritinib and olaparib in HGSOC PDX models. **A–E,** SCID beige mice were inoculated by intraperitoneal injection of disaggregated PDX tumors, with indicated gene alterations and HRD scores. When tumors reached 0.3–0.5 cm^2 in cross-sectional area by transabdominal ultrasound, mice were treated daily by oral gavage with 100 mg/kg ceritinib, 50 mg/kg olaparib, or 100 mg/kg ceritinib + 50 mg/kg olaparib for 9 weeks or until tumor dimensions determined by ultrasound indicated that tumors were greater than or equal to 10% of body weight or if humane endpoints were met. Tumor areas were monitored weekly by transabdominal ultrasound. Coloring in the plot indicates drug arm. Predicted lines are the average estimates computed from the statistical model fixed effects, relative to the arm-specific baseline estimate. Shading indicates 95% confidence intervals. The *P* values are provided in Supplementary Table S3. The number of mice under observation at each time point for each arm is indicated below the *x*-axis as a function of time, where text color indicates drug arm.

known to increase the production of ROS. Notably, complex I is emerging as a therapeutic target to treat malignancies (31). For example, the complex I inhibitor IACS-010759, which we show also synergized with olaparib, has antineoplastic activity in preclinical models and was well tolerated with preliminary evidence of antitumor activity in patients (44–48).

Importantly, we also show that ROS-induced DNA damage contributes to ceritinib's antiproliferative effects as demonstrated by the fact that the antioxidant N-acetylcysteine inhibited ceritinib's antiproliferative effects and that the ATR inhibitor berzosertib increased ceritinib cytotoxicity. In addition, XRCC1 depletion sensitized to ceritinib, indicating that the DNA damage that contributes to ceritinib

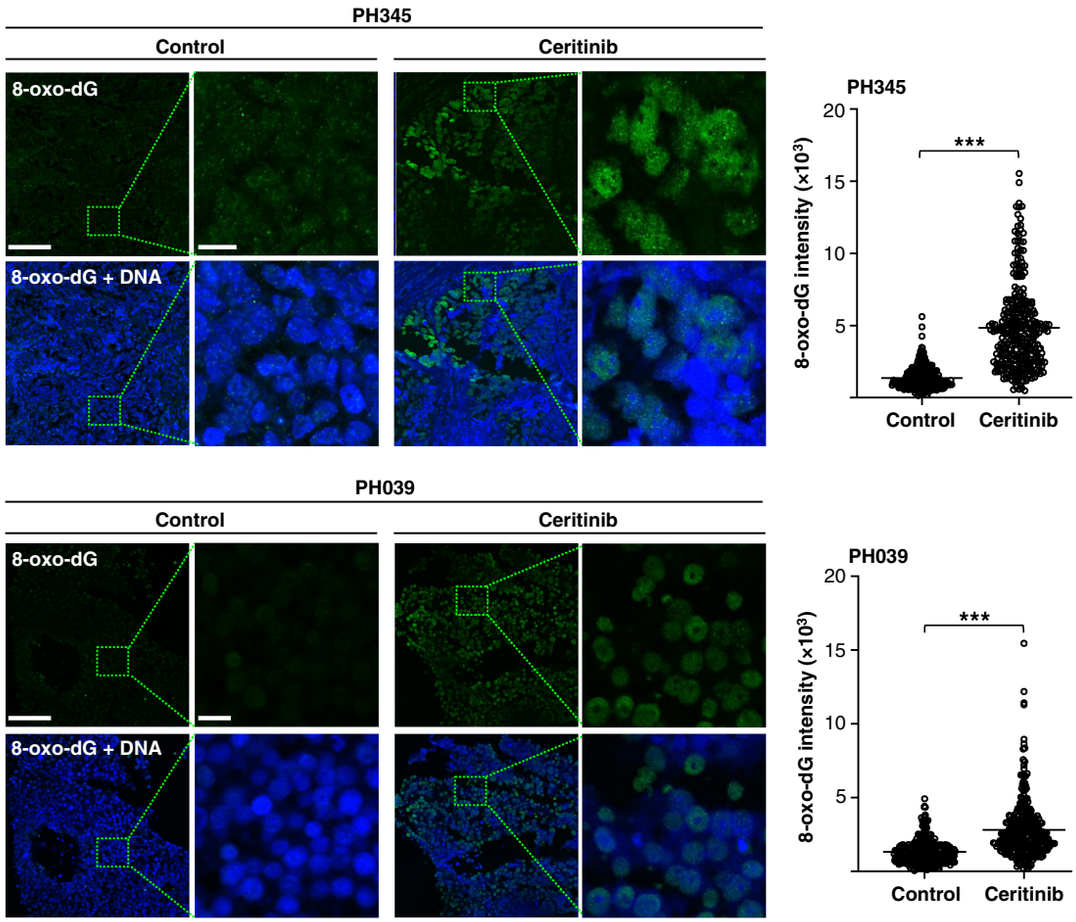

Figure 6.

Ceritinib induces oxidative DNA damage in HGSOC PDX tumors. Tumor specimens from mice bearing PDX models PH345 and PH039 that were treated with vehicle control or ceritinib were immunostained for 8-oxo-dG (green) and counterstained for DNA (blue) and analyzed by confocal microscopy. Representative confocal images of three tumor specimens from three different mice per model are shown; scale bars, 100 μm for low magnification images and 5 μm for high magnification images. Quantification of fluorescence intensity (right) was performed using ImageJ software (NIH). Three hundred cells (100 cells/tumor specimen) per PDX model were quantified. Error bars are mean ±SEM. ***, $P < 0.001$ relative to vehicle control, unpaired Student t test.

cytotoxicity is repaired by the BER/single-strand break DNA repair pathway, a PARP-dependent pathway that is one of the major repair pathways for hydroxyl radical-induced DNA damage (55). Consistent with the ability of ceritinib to inflict DNA damage that activates PARP and that is repaired in a PARP-dependent manner, we found that the addition of a PARPi, synergized with ceritinib. However, there may be an additional mechanism at work. In agreement with a previous report (43), we found that olaparib alone induced ROS (**Fig. 4A**), possibly due to its ability to upregulate NADPH oxidase isoforms that produce intracellular ROS. Moreover, as shown in **Fig. 4A–D**, combining ceritinib with olaparib further increased ROS levels and oxidative DNA damage, as well as PARP trapping on chromatin. Taken together, these findings support a model in which ceritinib and olaparib, alone and together, produce ROS-induced DNA damage. Because this damage is repaired, at least in part, by PARP-dependent repair pathways, the PARPi then inhibits DNA repair and traps PARP on chromatin, leading to cell killing and tumor regression (**Fig. 7**).

Earlier efforts to combine PARPis with agents that induce lesions repaired by BER have been hampered by toxicities (56). In contrast, we have observed that combining a PARPi with ceritinib had increased activity in multiple ovarian cancer PDX models with little additional toxicity. Moreover, the ceritinib + olaparib combination appears particularly effective in PARPi-responsive tumors. These observations, if confirmed in additional preclinical studies, have potential clinical implications. Even though PARPis have extended PFS in HGOSC, especially for tumors with HR defects (3, 7), most tumors eventually acquire PARPi resistance (57). The present preclinical findings suggest that a ceritinib + PARPi combination could be considered for clinical assessment as a possible way to enhance the activity of PARPis in HGSOCs, especially in tumors with preexisting HR defects that confer PARPi sensitivity, to delay or prevent the emergence of PARPi-resistant disease.

Authors' Disclosures

G. Vasmatzis reports other support from WholeGenome LLC outside the submitted work. A.L. Oberg reports grants from NCI during the conduct of the study. S.H. Kaufmann reports grants from National Cancer Institute during the conduct of the study; as well as reports nonfinancial support from Clovis Oncology outside the submitted work; as well as a patent for mechanisms of resistance to PARP inhibitors issued. A.S. Mansfield reports grants from Novartis during the conduct of the study; and other support from Genentech, Abbvie, BMS, Janssen, and grants from Mark Foundation, NIH, Department of Defense, and other support from Shanghai Roche

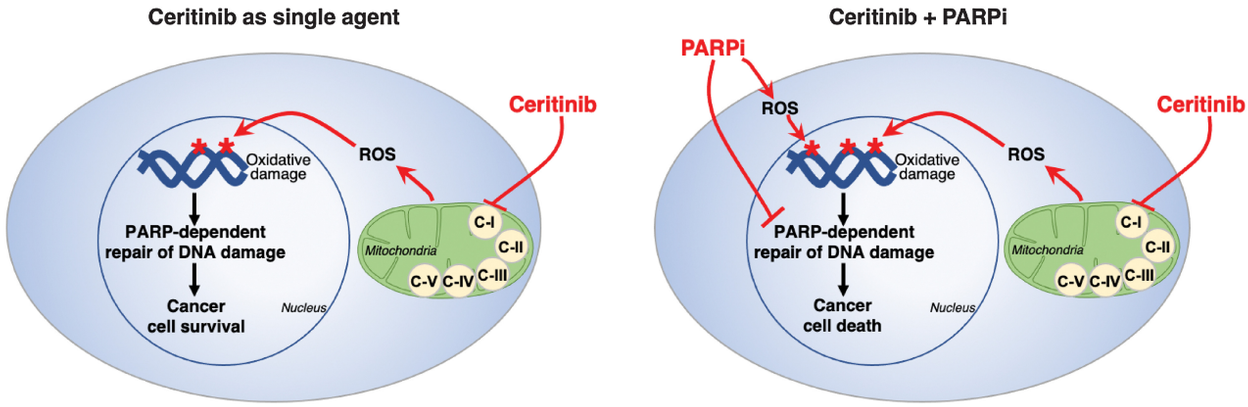

Figure 7.

Model for the ceritinib + PARPi synergy in HGSOC cells. In the context of single-agent ceritinib (left), ceritinib-induced oxidative DNA damage, resulting from increased ROS levels due to inhibition of mitochondrial respiration (OXPHOS) by targeting complex I, is repaired via PARP-dependent repair pathways. In the context of PARPi + ceritinib (right), repair of ceritinib- and PARPi-induced oxidative DNA damage is inhibited by PARPi, leading to cancer cell death.

Pharmaceuticals outside the submitted work; and nonremunerated director of the Mesothelioma Applied Research Foundation. S. Weroha reports personal fees from Kiyatec outside the submitted work. L.M. Karnitz reports grants from NIH during the conduct of the study. No disclosures were reported by the other authors.

Authors' Contributions

A. Kanakkanthara: Conceptualization, resources, data curation, formal analysis, supervision, funding acquisition, investigation, methodology, writing–original draft, project administration, writing–review and editing. **X. Hou:** Resources, data curation, formal analysis, investigation, methodology, writing–review and editing. **T.L. Ekstrom:** Resources, data curation, investigation, methodology, writing–review and editing. **V. Zanfagnin:** Conceptualization, resources, funding acquisition, investigation, writing–review and editing. **A.M. Huehls:** Resources, data curation, validation, investigation, writing–review and editing. **R.L. Kelly:** Resources, validation, investigation, writing–review and editing. **H. Ding:** Investigation, writing–review and editing. **M.C. Larson:** Formal analysis, visualization, methodology, writing–review and editing. **G. Vasmatzis:** Resources, data curation, formal analysis, writing–review and editing. **A.L. Oberg:** Data curation, formal analysis, supervision, validation, visualization, methodology, writing–review and editing. **S.H. Kaufmann:** Resources, funding acquisition, writing–review and editing. **A.S. Mansfield:** Conceptualization, funding acquisition, writing–review and editing. **S.J. Weroha:** Conceptualization, resources, data curation, formal analysis, supervision, funding acquisition, investigation, methodology, writing–original draft. **L.M. Karnitz:** Conceptualization, resources, data curation, supervision, funding acquisition, investigation, writing–original draft, project administration, writing–review and editing.

Acknowledgments

This work was supported by NIH (R01 CA194498 to L.M. Karnitz), a Mayo Clinic Ovarian Cancer SPORE Developmental Award (P50 CA136393 to L.M. Karnitz and A. Kanakkanthara), a Mayo Clinic Ovarian Cancer SPORE Career Enhancement Award (P50 CA136393 to A. Kanakkanthara), a Foundation for Women's Cancer Genentech Ovarian Cancer Young Investigator Career Development Award (to A. Kanakkanthara), and a Wallace and Evelyn Simmers Career Development Award for Ovarian Cancer Research (to A. Kanakkanthara), a Minnesota Ovarian Cancer Alliance grant (to V. Zanfagnin), Ovarian Cancer Research Alliance Liz Tilberis Early Career Award (to S.J. Weroha), and funding from the Novartis Investigator Initiated Studies Program (to A.S. Mansfield and S.J. Weroha). The authors also thank Paul Haluska and Marc A. Becker for providing RNA-seq data.

The publication costs of this article were defrayed in part by the payment of publication fees. Therefore, and solely to indicate this fact, this article is hereby marked "advertisement" in accordance with 18 USC section 1734.

Note

Supplementary data for this article are available at Cancer Research Online (http://cancerres.aacrjournals.org/).

Received March 5, 2021; revised August 5, 2021; accepted November 15, 2021; published first November 22, 2021.

References

1. Bowtell DD, Bohm S, Ahmed AA, Aspuria PJ, Bast RC, Beral V, et al. Rethinking ovarian cancer II: reducing mortality from high-grade serous ovarian cancer. Nat Rev Cancer 2015;15:668–79.
2. Cancer Genome Atlas Research Network. Integrated genomic analyses of ovarian carcinoma. Nature 2011;474:609–15.
3. Konstantinopoulos PA, Ceccaldi R, Shapiro GI, D'Andrea AD. Homologous recombination deficiency: exploiting the fundamental vulnerability of ovarian cancer. Cancer Discov 2015;5:1137–54.
4. Pujade-Lauraine E, Banerjee S, Pignata S. Management of platinum-resistant, relapsed epithelial ovarian cancer and new drug perspectives. J Clin Oncol 2019; 37:2437–48.
5. Ray Chaudhuri A, Nussenzweig A. The multifaceted roles of PARP1 in DNA repair and chromatin remodelling. Nat Rev Mol Cell Biol 2017;18:610–21.
6. Mirza MR, Coleman RL, Gonzalez-Martin A, Moore KN, Colombo N, Ray-Coquard I, et al. The forefront of ovarian cancer therapy: update on PARP inhibitors. Ann Oncol 2020;31:1148–59.
7. Slade D. PARP and PARG inhibitors in cancer treatment. Genes Dev 2020;34: 360–94.
8. Kaufman B, Shapira-Frommer R, Schmutzler RK, Audeh MW, Friedlander M, Balmana J, et al. Olaparib monotherapy in patients with advanced cancer and a germline BRCA1/2 mutation. J Clin Oncol 2015; 33:244–50.
9. Audeh MW, Carmichael J, Penson RT, Friedlander M, Powell B, Bell-McGuinn KM, et al. Oral poly(ADP-ribose) polymerase inhibitor olaparib in patients with BRCA1 or BRCA2 mutations and recurrent ovarian cancer: a proof-of-concept trial. Lancet 2010;376:245–51.
10. Gelmon KA, Tischkowitz M, Mackay H, Swenerton K, Robidoux A, Tonkin K, et al. Olaparib in patients with recurrent high-grade serous or poorly differentiated ovarian carcinoma or triple-negative breast cancer: a phase 2, multicentre, open-label, non-randomised study. Lancet Oncol 2011;12:852–61.
11. Mirza MR, Monk BJ, Herrstedt J, Oza AM, Mahner S, Redondo A, et al. Niraparib maintenance therapy in platinum-sensitive, recurrent ovarian cancer. N Engl J Med 2016;375:2154–64.
12. Shaw AT, Engelman JA. ALK in lung cancer: past, present, and future. J Clin Oncol 2013;31:1105–11.

13. Golding B, Luu A, Jones R, Viloria-Petit AM. The function and therapeutic targeting of anaplastic lymphoma kinase (ALK) in non–small cell lung cancer (NSCLC). Mol Cancer 2018;17:52.
14. Huntoon CJ, Flatten KS, Wahner Hendrickson AE, Huehls AM, Sutor SL, Kaufmann SH, et al. ATR inhibition broadly sensitizes ovarian cancer cells to chemotherapy independent of BRCA status. Cancer Res 2013;73:3683–91.
15. Chou TC, Talalay P. Quantitative analysis of dose-effect relationships: the combined effects of multiple drugs or enzyme inhibitors. Adv Enzyme Regul 1984;22:27–55.
16. Kanakkanthara A, Kurmi K, Ekstrom TL, Hou X, Purfeerst ER, Heinzen EP, et al. BRCA1 deficiency upregulates NNMT, which reprograms metabolism and sensitizes ovarian cancer cells to mitochondrial metabolic targeting agents. Cancer Res 2019;79:5920–9.
17. Murai J, Huang SY, Das BB, Renaud A, Zhang Y, Doroshow JH, et al. Trapping of PARP1 and PARP2 by clinical PARP inhibitors. Cancer Res 2012;72:5588–99.
18. Weroha SJ, Becker MA, Enderica-Gonzalez S, Harrington SC, Oberg AL, Maurer MJ, et al. Tumorgrafts as *in vivo* surrogates for women with ovarian cancer. Clin Cancer Res 2014;20:1288–97.
19. Butler KA, Hou X, Becker MA, Zanfagnin V, Enderica-Gonzalez S, Visscher D, et al. Prevention of human lymphoproliferative tumor formation in ovarian cancer patient-derived xenografts. Neoplasia 2017;19:628–36.
20. Oberg AL, Heinzen EP, Hou X, Al Hilli MM, Hurley RM, Wahner Hendrickson AE, et al. Statistical analysis of comparative tumor growth repeated measures experiments in the ovarian cancer patient derived xenograft (PDX) setting. Sci Rep 2021;11:8076.
21. R Core Team (2021). R: A language and environment for statistical computing. R Foundation for Statistical Computing, Vienna, Austria. Available at: https://www.R-project.org/.
22. Mitra AK, Davis DA, Tomar S, Roy L, Gurler H, Xie J, et al. *In vivo* tumor growth of high-grade serous ovarian cancer cell lines. Gynecol Oncol 2015;138:372–7.
23. Nakanishi K, Cavallo F, Brunet E, Jasin M. Homologous recombination assay for interstrand cross-link repair. Methods Mol Biol 2011;745:283–91.
24. Kuenzi BM, Rix LLR, Stewart PA, Fang B, Kinose F, Bryant AT, et al. Polypharmacology-based ceritinib repurposing using integrated functional proteomics. Nat Chem Biol 2017;13:1222–31.
25. Available from: https://www.proteinatlas.org/ENSG00000171094-ALK/cell. The human protein atlas: ALK protein levels in cell lines.
26. Carneiro BA, Pamarthy S, Shah AN, Sagar V, Unno K, Han H, et al. Anaplastic lymphoma kinase mutation (ALK F1174C) in small cell carcinoma of the prostate and molecular response to alectinib. Clin Cancer Res 2018;24:2732–9.
27. Zhang J, Salminen A, Yang X, Luo Y, Wu QG, White M, et al. Effects of 31 FDA approved small-molecule kinase inhibitors on isolated rat liver mitochondria. Arch Toxicol 2017;91:2921–38.
28. Turrens JF. Mitochondrial formation of reactive oxygen species. J Physiol 2003; 552:335–44.
29. Murphy MP. How mitochondria produce reactive oxygen species. Biochem J 2009;417:1–13.
30. Brand MD. The sites and topology of mitochondrial superoxide production. Exp Gerontol 2010;45:466–72.
31. Ashton TM, McKenna WG, Kunz-Schughart LA, Higgins GS. Oxidative phosphorylation as an emerging target in cancer therapy. Clin Cancer Res 2018;24:2482–90.
32. Cho BC, Kim DW, Bearz A, Laurie SA, McKeage M, Borra G, et al. ASCEND-8: a randomized phase 1 study of ceritinib, 450 mg or 600 mg, taken with a low-fat meal versus 750 mg in fasted state in patients with anaplastic lymphoma kinase (ALK)-rearranged metastatic non–small cell lung cancer (NSCLC). J Thorac Oncol 2017;12:1357–67.
33. Ward IM, Chen J. Histone H2AX is phosphorylated in an ATR-dependent manner in response to replicational stress. J Biol Chem 2001;276:47759–62.
34. Podhorecka M, Skladanowski A, Bozko P. H2AX Phosphorylation: its role in DNA damage response and cancer therapy. J Nucleic Acids 2010;2010:920161.
35. Wei H, Yu X. Functions of PARylation in DNA damage repair pathways. Genomics Proteomics Bioinformatics 2016;14:131–9.
36. Gibson BA, Kraus WL. New insights into the molecular and cellular functions of poly(ADP-ribose) and PARPs. Nat Rev Mol Cell Biol 2012;13:411–24.
37. Redon CE, Nakamura AJ, Zhang YW, Ji JJ, Bonner WM, Kinders RJ, et al. Histone gammaH2AX and poly(ADP-ribose) as clinical pharmacodynamic biomarkers. Clin Cancer Res 2010;16:4532–42.
38. Davidovic L, Vodenicharov M, Affar EB, Poirier GG. Importance of poly(ADP-ribose) glycohydrolase in the control of poly(ADP-ribose) metabolism. Exp Cell Res 2001;268:7–13.
39. Li N, Chen J. ADP-ribosylation: activation, recognition, and removal. Mol Cells 2014;37:9–16.
40. Karnitz LM, Zou L. Molecular pathways: targeting ATR in cancer therapy. Clin Cancer Res 2015;21:4780–5.
41. Reaper PM, Griffiths MR, Long JM, Charrier JD, MacCormick S, Charlton PA, et al. Selective killing of ATM- or p53-deficient cancer cells through inhibition of ATR. Nat Chem Biol 2011;7:428–30.
42. Hou D, Liu Z, Xu X, Liu Q, Zhang X, Kong B, et al. Increased oxidative stress mediates the antitumor effect of PARP inhibition in ovarian cancer. Redox Biol 2018;17:99–111.
43. Santiago-O'Farrill JM, Weroha SJ, Hou X, Oberg AL, Heinzen EP, Maurer MJ, et al. Poly(adenosine diphosphate ribose) polymerase inhibitors induce autophagy-mediated drug resistance in ovarian cancer cells, xenografts, and patient-derived xenograft models. Cancer 2020;126:894–907.
44. Molina JR, Sun Y, Protopopova M, Gera S, Bandi M, Bristow C, et al. An inhibitor of oxidative phosphorylation exploits cancer vulnerability. Nat Med 2018;24: 1036–46.
45. Vyas A, Harbison RA, Faden DL, Kubik M, Palmer D, Zhang Q, et al. Recurrent human papillomavirus-related head and neck cancer undergoes metabolic reprogramming and is driven by oxidative phosphorylation. Clin Cancer Res 2021:27:6250–64.
46. Stuani L, Sabatier M, Saland E, Cognet G, Poupin N, Bosc C, et al. Mitochondrial metabolism supports resistance to IDH mutant inhibitors in acute myeloid leukemia. J Exp Med 2021;218:e20200924.
47. Fischer GM, Jalali A, Kircher DA, Lee WC, McQuade JL, Haydu LE, et al. Molecular profiling reveals unique immune and metabolic features of melanoma brain metastases. Cancer Discov 2019;9:628–45.
48. Vashisht Gopal YN, Gammon S, Prasad R, Knighton B, Pisaneschi F, Roszik J, et al. A novel mitochondrial inhibitor blocks MAPK pathway and overcomes MAPK inhibitor resistance in melanoma. Clin Cancer Res 2019;25:6429–42.
49. Friboulet L, Li N, Katayama R, Lee CC, Gainor JF, Crystal AS, et al. The ALK inhibitor ceritinib overcomes crizotinib resistance in non–small cell lung cancer. Cancer Discov 2014;4:662–73.
50. Min A, Im SA, Yoon YK, Song SH, Nam HJ, Hur HS, et al. RAD51C-deficient cancer cells are highly sensitive to the PARP inhibitor olaparib. Mol Cancer Ther 2013;12:865–77.
51. Maifrede S, Nieborowska-Skorska M, Sullivan-Reed K, Dasgupta Y, Podszywalow-Bartnicka P, Le BV, et al. Tyrosine kinase inhibitor-induced defects in DNA repair sensitize FLT3(ITD)-positive leukemia cells to PARP1 inhibitors. Blood 2018;132:67–77.
52. Balaji K, Vijayaraghavan S, Diao L, Tong P, Fan Y, Carey JP, et al. AXL inhibition suppresses the DNA damage response and sensitizes cells to PARP inhibition in multiple cancers. Mol Cancer Res 2017;15:45–58.
53. Kaplan AR, Gueble SE, Liu Y, Oeck S, Kim H, Yun Z, et al. Cediranib suppresses homology-directed DNA repair through downregulation of BRCA1/2 and RAD51. Sci Transl Med 2019;11:eaav4508.
54. Liu JF, Barry WT, Birrer M, Lee JM, Buckanovich RJ, Fleming GF, et al. Combination cediranib and olaparib versus olaparib alone for women with recurrent platinum-sensitive ovarian cancer: a randomised phase 2 study. Lancet Oncol 2014;15:1207–14.
55. Abbotts R, Wilson DM III. Coordination of DNA single strand break repair. Free Radic Biol Med 2017;107:228–44.
56. Veneris JT, Matulonis UA, Liu JF, Konstantinopoulos PA. Choosing wisely: selecting PARP inhibitor combinations to promote antitumor immune responses beyond BRCA mutations. Gynecol Oncol 2020;156:488–97.
57. Noordermeer SM, van Attikum H. PARP inhibitor resistance: a tug-of-war in BRCA-mutated cells. Trends Cell Biol 2019;29:820–34.